Japanese Journal of Applied Physics

REGULAR PAPERS

Structural and magnetic characterization of Mn/NiFe bilayers with ion-beam-assisted deposition

To cite this article: Chun-Hsien Wu *et al* 2018 *Jpn. J. Appl. Phys.* **57** 01AC04

Japanese Journal of Applied Physics **57**, 01AC04 (2018)
https://doi.org/10.7567/JJAP.57.01AC04

REGULAR PAPER

Structural and magnetic characterization of Mn/NiFe bilayers with ion-beam-assisted deposition

Chun-Hsien Wu[1†], Chao Zheng[2†], Chun-Cheng Chiu[1], Palash Kumar Manna[3], Johan van Lierop[3*], Ko-Wei Lin[1*], and Philip W. T. Pong[2*]

[1]*Department of Materials Science and Engineering, National Chung Hsing University, Taichung 402, Taiwan*
[2]*Department of Electrical and Electronic Engineering, The University of Hong Kong, Hong Kong*
[3]*Department of Physics and Astronomy, University of Manitoba, Winnipeg, MB R3T 2N2, Canada*

*E-mail: johan@physics.umanitoba.ca; kwlin@dragon.nchu.edu.tw; ppong@eee.hku.hk
†These authors contributed equally to this work.

Received May 15, 2017; revised September 1, 2017; accepted September 28, 2017; published online November 17, 2017

The exchange bias effect in ferromagnetic (FM)/antiferromagnetic (AF) bilayer structures has been widely investigated because its underlying principle is critical for spintronic applications. In this work, the effect of Ar^+ beam bombardment on the microstructural and magnetic properties of the Mn/NiFe thin films was investigated. The in-situ Ar^+ bombardment nontrivially promoted the Mn/NiFe intermixing and facilitated the formation of the FeMn phase, accompanied by a remarkable reduction of Mn and NiFe layer thickness. The enhanced Mn/NiFe intermixing greatly disordered the interfacial spins, inhibiting the interfacial exchange coupling and giving rise to a significant decrease of the exchange bias field (H_{ex}). The facilitated Mn/NiFe intermixing effect also dramatically degraded the magnetocrystalline anisotropy of the NiFe crystallites, leading to a notable suppression of the coercivity (H_c). These results indicate that both the exchange bias and coercivity of the Mn/NiFe bilayers can be directly affected by the in-situ Ar^+ bombardment, offering an effective way to modify the magnetism of the exchange-bias systems.

1. Introduction

The exchange bias phenomenon in ferromagnetic (FM)/antiferromagnetic (AF) bilayer structures has been widely investigated because its underlying principle is vital for spintronic applications.[1–4] The microstructural and magnetic characteristics of the FM/AF bilayers can be changed by a variety of methods, including annealing,[5] ion-beam bombardment,[6] and field cooling.[7] Among these methods, the ion-beam bombardment is an effective technique to modify the microstructural and compositional features of the FM/AF bilayers by altering crystallographic orientations,[8] changing grain sizes,[6] facilitating interlayer diffusion,[3,9] and so on. The altered microstructural and compositional properties can nontrivially influence the exchange bias and coercivity of the FM/AF bilayers,[2–4,8,10,11] revealing the critical role of the ion-beam bombardment in modifying the magnetism of the FM/AF bilayers.

As a common AF material, Mn is widely used in the exchange biased structures.[12–20] The published works have demonstrated the effect of the oxidization of Mn,[16,21] the Mn doping,[22–24] and the Mn diffusion[15,25,26] on the exchange-biased thin films. However, the influence of the ion-beam bombardment on Mn/NiFe bilayers has not yet been reported. In this work, the authors studied the changes of microstructural and compositional properties induced by the ion-beam bombardment and discussed their consequent effects on the magnetism of the exchange-biased Mn/NiFe bilayers.

2. Experimental methods

The Mn/NiFe bilayers were deposited on amorphous SiO_2 substrates by using a dual ion-beam sputtering system.[27,28] The base pressure of the chamber was 4×10^{-6} Torr. The bilayer samples were either prepared without (as-deposited) or with (bombarded) Ar^+ bombardment during the deposition of the Mn layer. A quartz oscillator was used to monitor the deposition process. The pressure of the chamber was stabilized at 5×10^{-4} Torr during the deposition. For the as-deposited samples, an Ar^+ beam from a Kaufman ion source was focused onto a commercial NiFe or Mn target in order to deposit the bottom NiFe or top Mn layer. The operating voltage and current of the Kaufman ion source were stabilized at 804 V and 7.5 mA, respectively. The NiFe and Mn layers with thicknesse of 23.1 and 35.2 nm were deposited at the deposition rate of approximately 4.6 and 2.9 nm/min, respectively. The deposition times of the NiFe and Mn layers were 5 and 12 min, respectively. For the bombarded samples, the NiFe layer with thickness of 23.1 nm was deposited at the same deposition rate of approximately 4.6 nm/min and the deposition time was 5 min as well. After the deposition of the NiFe layer, an end-Hall ion source with an Ar^+ beam was utilized to in-situ bombard the substrate during the deposition of the Mn layer. The deposition time of the Mn layer was 12 min. The operating voltage (V_{EH}) of the end-Hall ion source was maintained at 70 V during the ion-beam bombardment process. The microstructural properties of the prepared samples were characterized with a JEOL JEM-2010 transmission electron microscope (TEM) operating at 200 kV. A Bruker AXS D8 Advance system was used to acquire X-ray diffraction (XRD) patterns. The X-ray photoelectron spectroscopy (XPS) investigations were conducted on a PHI 5000 VersaProbe. Magnetic hysteresis loop measurements were performed in a superconducting quantum interference device (SQUID; Quantum Design MPMS) where a cooling field of 0.1 T (1 kOe) was applied parallel to the sample plane. The zero-field-cooled (ZFC) and field-cooled (FC) curves were measured with an in-plane magnetic field of 10 mT (100 Oe) over a temperature range from 300 to 10 K.

3. Results and discussion

Microstructural properties of both the as-deposited and bombarded Mn/NiFe bilayers were investigated via TEM. As shown in the bright field TEM images [Figs. 1(a) and 1(b)], a columnar-like morphology was exhibited in the as-

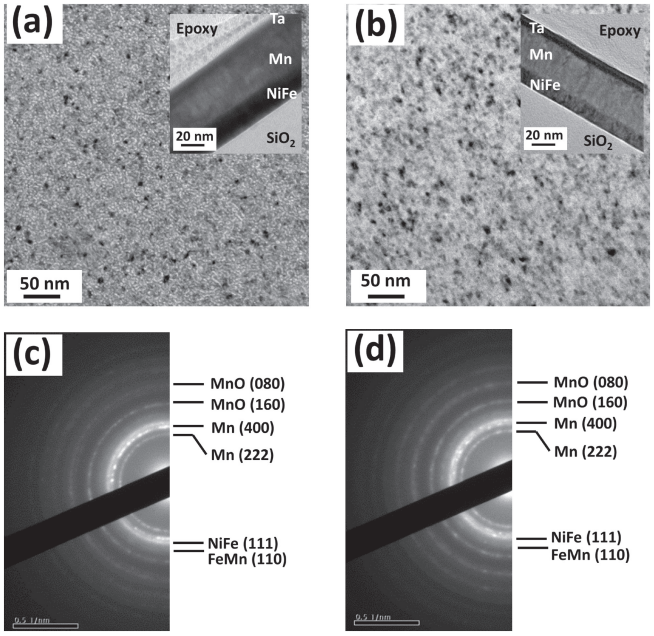

Fig. 1. TEM micrographs of the (a) as-deposited and (b) bombarded $Ta/Mn/NiFe/SiO_2$ thin films. Cross-sectional TEM images are shown in the insets of (a) and (b). SAED patterns of the as-deposited and bombarded thin films are shown in (c) and (d), respectively.

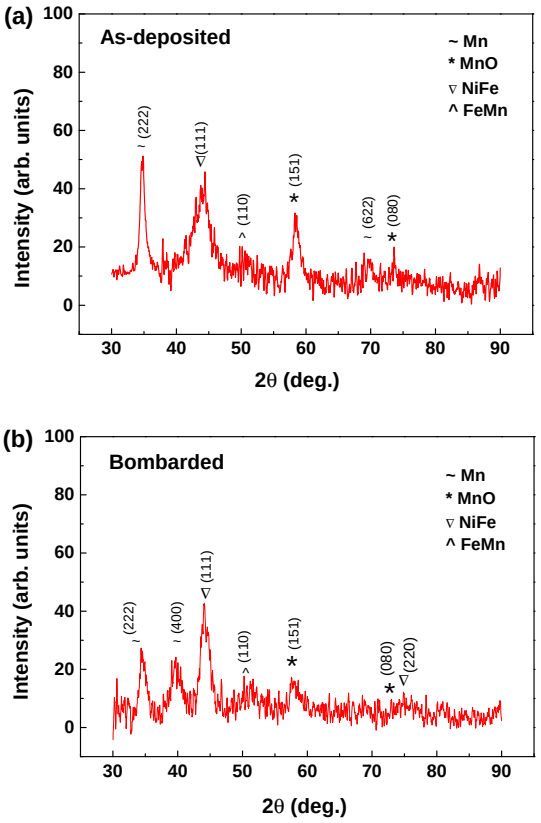

Fig. 2. (Color online) XRD spectra of the (a) as-deposited and (b) bombarded Mn/NiFe bilayers.

deposited bilayer and such morphology was absent in the bombarded one. Through in-situ Ar^+ bombardment during the deposition of the Mn layer, the thicknesses of the Mn and NiFe layers were greatly decreased to 27.1 and 11.8 nm [insets of Figs. 1(a) and 1(b)], respectively. This phenomenon was caused by the etching effect of the Ar^+ bombardment. When the deposition of the Mn layer started, the Ar ions generated from the end-Hall ion source could either transfer their momentums to the Mn atoms or penetrate into the NiFe layer and transfer their momentums to the Ni or Fe atoms. Therefore, both the Mn and NiFe layers were partially etched during the ion beam bombardment process, resulting in the reduction of thickness of the Mn and NiFe layers. The rough Mn/NiFe interfaces of both the as-deposited and bombarded layers indicated a nontrivial intermixing between the Mn and NiFe layers. To acquire more microstructural information, the selected area electron diffraction (SAED) patterns of the bilayers were analyzed, as demonstrated in Figs. 1(c) and 1(d). Both the as-deposited and bombarded bilayers revealed the major Mn phase and minor MnO phase, suggesting a slight oxidization of the Mn layer, which was probably caused by the residual oxygen in the chamber. The major Mn phase mainly exhibited (222) and (400) textures while the MnO phase showed a combination of (160) and (080) textures. Regarding the bombarded bilayer, the observation of bright diffraction spots in the NiFe(111) ring suggested the growth of NiFe grains. The intermixing between the Mn and NiFe layers also resulted in the formation of the FeMn phase.

XRD characterization was carried out to further investigate the effect of Ar^+ bombardment on the microstructural and compositional properties of the Mn/NiFe bilayers. As shown in Figs. 2(a) and 2(b), the diffraction peaks for the Mn, MnO, and FeMn phases were identified. For the as-deposited bilayer [Fig. 2(a)], both the Mn(222) and MnO(151) peaks were identified, which suggested the oxidization of the Mn layer. A relatively wide NiFe(111) peak was identified and a small FeMn(110) peak was present due to the intermixing effect. Compared to the as-deposited bilayer [Fig. 2(a)], the peak intensity of the MnO(151) for the bombarded bilayer [Fig. 2(b)] exhibited a notable decrease, indicating the reduction of oxidized phase in the Mn layer during ion beam bombardment process. Also, the integral peak intensity of the FeMn(110) texture became slightly larger, which was confirmed by the calculated ratio of integral peak intensity between the bombard and as-deposited layers of ~1.16. This phenomenon revealed that the intermixing effect was enhanced and an increasing amount of the FeMn phase was formed during ion beam bombardment. The bombarded bilayer also exhibited a much sharper NiFe(111) peak, indicating the growth of NiFe grains due to the in-situ Ar^+ bombardment. These characterizations are consistent with the discussed TEM and SAED results.

To further characterize the chemical composition of the as-deposited and bombarded bilayers, XPS measurements of the bilayers were investigated and their depth profile intensities were analyzed, as shown in Figs. 3(a) and 3(b). In Fig. 3(a), when the sputtering time (t_s) < 0.8 min, the intensity of Ta was larger that of Mn, Ni, Fe, and O, which revealed the formation of the Ta capping layer of the as-deposited specimen. After t_s of 0.8 min, the content of Mn exhibited a rapid increase, suggesting the detection of the Mn layer. The detection of the O signal confirmed the oxidization of the Mn layer at the Ta/Mn interface. After t_s of 7.0 min, the content of Mn started to decrease while that of Ni and Fe demonstrated a sharp growth, indicating the NiFe layer was

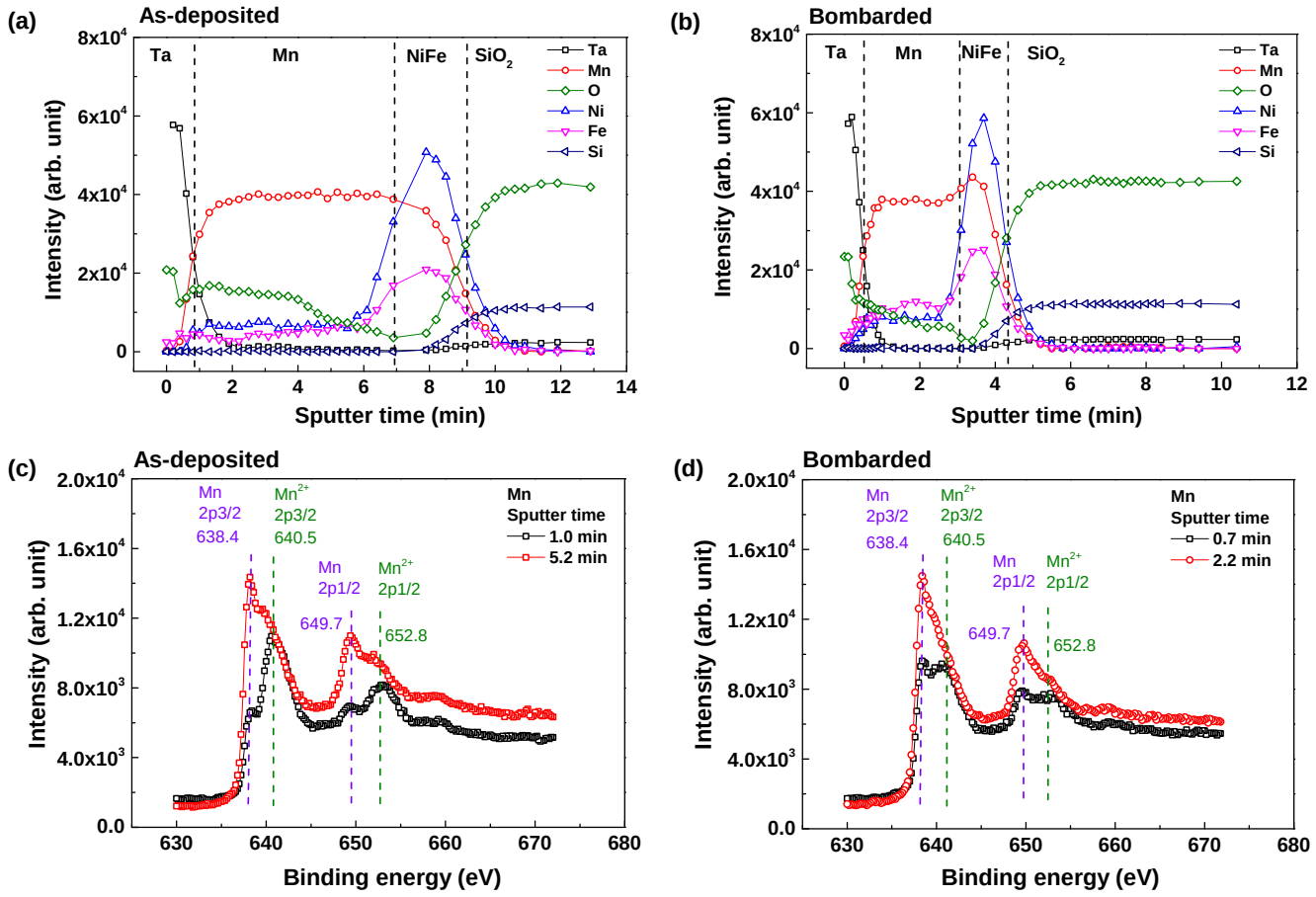

Fig. 3. (Color online) XPS depth profiles for the (a) as-deposited and (b) bombarded samples. The XPS spectra of Mn $2p_{3/2(1/2)}$ electrons for the as-deposited and bombarded samples are shown in (c) and (d), respectively.

detected. The relatively large Mn content in the NiFe layer was a result of the intermixing between the Mn and NiFe layers. In the bombarded sample [Fig. 3(b)], larger intensities of Ni and Fe were detected in the Mn layer as well as a larger Mn content was identified in the NiFe layer as compared to the as-deposited sample, which suggested the enhanced Mn/NiFe intermixing in the bombarded sample. These results confirm the oxidization of the Mn layer at the Ta/Mn interface and the enhancement of Mn/NiFe intermixing due to the Ar^+ bombardment.

To validate the formation of the oxidized state of Mn, XPS spectra of Mn $2p_{3/2(1/2)}$ electrons were analyzed for both the as-deposited [Fig. 3(c)] and bombarded samples [Fig. 3(d)]. For the as-deposited sample with t_s of 1.0 min [Fig. 3(c)], the major peaks at 640.5 and 652.8 eV indicated the emissions of Mn^{2+} ions in MnO while the subpeaks at 638.4 and 649.7 eV corresponded to the metallic Mn.[29] When t_s of 5.2 min, the Mn 2p peaks exhibited a significant growth and tended to overwhelm the Mn^{2+} 2p peaks, suggesting that the metallic Mn phase was dominant. This phenomenon was in line with the reduction of O content at t_s of 5.2 min, as demonstrated in the XPS depth profile of the as-deposited sample [Fig. 3(a)]. Similar results were revealed in the Mn 2p spectra for the bombarded sample [Fig. 3(d)]. At the Ta/Mn interface (t_s of 0.7 min), both the metallic and oxidized Mn phases were observed. When Ar^+ sputtered into the Mn layer, the Mn^{2+} peaks were dramatically suppressed, which suggested that the metallic Mn phase was dominant.

From the above microstructural and compositional investigation, we concluded that both the as-deposited and bombarded samples exhibited the intermixing effect between the Mn and NiFe layer as well as the slight oxidization of the Mn layer at the Ta/Mn interface. The in-situ Ar^+ bombardment nontrivially promoted the Mn/NiFe intermixing and facilitated the formation of the FeMn phase, accompanied by a remarkable reduction of Mn and NiFe layer thickness. These microstructural and compositional changes also influenced the magnetic properties of the as-deposited and bombarded Mn/NiFe bilayers, as investigated below.

To investigate the influence of the in-situ Ar^+ bombardment on the magnetic properties of the Mn/NiFe bilayers, the magnetic hysteresis loops were measured with an in-plane measuring magnetic field applied along the easy axis, as shown in Figs. 4(a) and 4(b). Compared to the as-deposited sample [Fig. 4(a)], the bombarded sample [Fig. 4(b)] exhibited a remarkable suppression of the normalized remanence (M_r/M_s). This phenomenon was likely originated from the enhanced intermixing between the Mn and NiFe layers, which led to the reduction of magnetocrystalline anisotropy of the NiFe crystallites and therefore resulted in the decrease of M_r/M_s.[30] The easy-axis exchange bias field (H_{ex}) and coercivity (H_c) were calculated at different temperatures, as shown in Fig. 4(c). The boosted H_{ex} and H_c at low temperatures (10, 20 K) was derived from the onset of exchange bias effect below the irreversibility temperature (T_{irr}). These results were confirmed by the FC/ZFC measure-

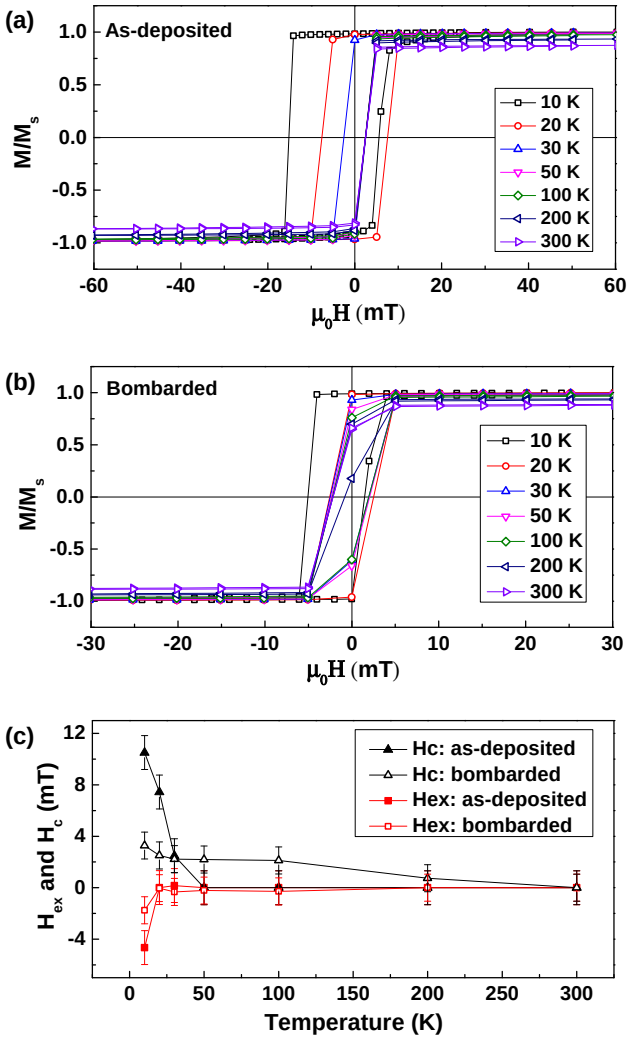

Fig. 4. (Color online) Hysteresis loops of the (a) as-deposited and (b) bombarded Mn/NiFe bilayers measured at various temperatures with an in-plane measuring magnetic field applied along the easy axis. Temperature dependence of the calculated exchange bias field (H_{ex}) and coercivity (H_c) is exhibited in (c).

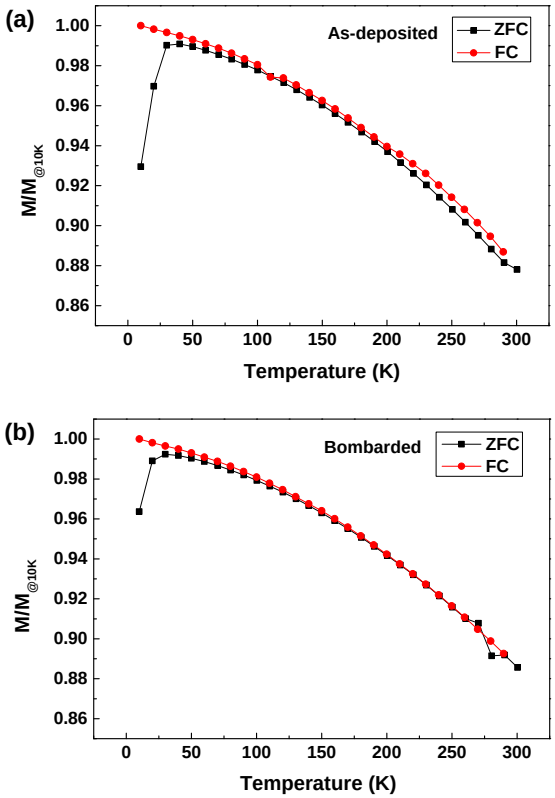

Fig. 5. (Color online) ZFC and FC curves for the (a) as-deposited and (b) bombarded samples, respectively. The measured magnetization (M) is normalized by the FC magnetization at 10 K ($M_{FC@10K}$).

ments [Figs. 5(a) and 5(b)] where the FC and ZFC curves started to diverge below 30 K, indicating similar T_{irr} values (~30 K) for the as-deposited and bombarded samples. At low temperatures (10, 20 K), the as-deposited sample revealed relatively large H_{ex} and H_c while the bombarded sample showed the significantly suppressed H_{ex} and H_c. The notable decrease of H_{ex} was attributed to the promotion of spin misalignment at the FM/AF interface induced by the Ar^+ bombardment. The disordered interfacial spins greatly inhibited the interfacial exchange coupling and resulted in a significant decrease of H_{ex}.[31] The in-situ Ar^+ bombardment also facilitated the Mn/NiFe intermixing effect, which dramatically reduced the magnetocrystalline anisotropy of the NiFe crystallites and gave rise to a suppressed H_c.[30]

4. Conclusions

In this work, the effect of Ar^+ ion beam bombardment on the microstructural and magnetic properties of the Mn/NiFe thin films was investigated. The in-situ Ar^+ bombardment during the deposition of the Mn layer can notably promote the Mn/NiFe intermixing and facilitate the formation of the FeMn phase accompanied by a remarkable reduction of Mn and NiFe thicknesses. The enhanced Mn/NiFe intermixing greatly disordered the interfacial spins, inhibiting the interfacial exchange coupling and giving rise to a significant decrease of H_{ex}. The facilitated Mn/NiFe intermixing effect also dramatically degraded the magnetocrystalline anisotropy of the NiFe crystallites, leading to a notable suppression of H_c. These results indicate that both the exchange bias and coercivity of the Mn/NiFe bilayers can be directly affected by the in-situ Ar^+ bombardment, offering an effective way to modify the magnetism of the exchange-bias systems.

Acknowledgements

This work was supported in part by the MOST of Taiwan, the NSERC and CFI of Canada, and the Seed Funding Program for Basic Research and Small Project Funding Program from the University of Hong Kong, ITF Tier 3 funding (ITS/104/13, ITS/214/14), and University Grants Committee of Hong Kong (Contract No. AoE/P-04/08).

1) J. van Lierop, B. Southern, K.-W. Lin, Z.-Y. Guo, C. Harland, R. Rosenberg, and J. Freeland, Phys. Rev. B **76**, 224432 (2007).
2) J. van Lierop, K.-W. Lin, J.-Y. Guo, H. Ouyang, and B. Southern, Phys. Rev. B **75**, 134409 (2007).
3) C. Zheng, K.-W. Lin, C.-H. Liu, H.-F. Hsu, C.-W. Leung, W.-H. Chen, T.-H. Wu, R. D. Desautels, J. van Lierop, and P. W. Pong, Vacuum **118**, 85 (2015).
4) C. Zheng, T.-C. Lan, C. Shueh, R. D. Desautels, J. van Lierop, K.-W. Lin, and P. W. Pong, Jpn. J. Appl. Phys. **53**, 06JB03 (2014).
5) G. Li, C. W. Leung, Y.-C. Chen, K.-W. Lin, A.-C. Sun, J.-H. Hsu, and P. W. T. Pong, Microelectron. Eng. **110**, 241 (2013).
6) K.-W. Lin, M. Mirza, C. Shueh, H.-R. Huang, H.-F. Hsu, and J. van Lierop, Appl. Phys. Lett. **100**, 122409 (2012).

7) X. Li, K.-W. Lin, H.-Y. Liu, D.-H. Wei, G. Li, and P. Pong, Thin Solid Films **570**, 383 (2014).
8) C. Shueh, D. L. Cortie, F. Klose, J. Van Lierop, and K. W. Lin, IEEE Trans. Magn. **48**, 2892 (2012).
9) C.-H. Su, S.-C. Lo, J. Van Lierop, K.-W. Lin, and H. Ouyang, J. Appl. Phys. **105**, 07C316 (2009).
10) C. Shueh, P. S. Chen, D. Cortie, F. Klose, W. C. Chen, T. H. Wu, J. van Lierop, and K. W. Lin, Jpn. J. Appl. Phys. **51**, 11PG02 (2012).
11) L.-X. Ye, C.-M. Lee, J.-W. Syu, Y.-R. Wang, K.-W. Lin, Y.-H. Chang, and T. Wu, IEEE Trans. Magn. **44**, 3601 (2008).
12) G. L. Causer, P. K. Manna, C. C. Chiu, J. van Lierop, M. Ionescu, K. W. Lin, and F. Klose, Nucl. Instrum. Methods Phys. Res., Sect. B **409**, 121 (2017).
13) S. S. Lee, D. G. Hwang, and G. Y. Ahn, J. Korean Phys. Soc. **34**, 280 (1999).
14) J. B. Youssef, D. Spenato, H. L. Gall, and J. Ostoréro, J. Appl. Phys. **91**, 7239 (2002).
15) S.-S. Lee, B.-K. Kim, J.-Y. Lee, D.-G. Hwang, S.-W. Kim, M.-Y. Kim, J.-Y. Hwang, and J.-R. Rhee, J. Appl. Phys. **95**, 7525 (2004).
16) K.-W. Lin, J.-Y. Guo, T.-J. Chen, H. Ouyang, E. Vass, and J. van Lierop, J. Appl. Phys. **104**, 123908 (2008).
17) B. Dai, Y. Lei, X. Shao, and J. Ni, J. Alloys Compd. **490**, 427 (2010).
18) S. Laureti, D. Peddis, L. Del Bianco, A. Testa, G. Varvaro, E. Agostinelli, C. Binns, S. Baker, M. Qureshi, and D. Fiorani, J. Magn. Magn. Mater. **324**, 3503 (2012).
19) A. El Bahoui, C. Genevois, J. Juraszek, C. Bordel, and D. Ledue, Physica B **416**, 45 (2013).
20) C.-H. Liu, C. Shueh, T.-C. Lan, K.-W. Lin, W.-C. Chen, T.-H. Wu, R. D. Desautels, and J. van Lierop, J. Korean Phys. Soc. **62**, 1958 (2013).
21) X. Wang and Y. Li, J. Am. Chem. Soc. **124**, 2880 (2002).
22) R. K. Zheng, H. Liu, X. X. Zhang, V. A. L. Roy, and A. B. Djurišić, Appl. Phys. Lett. **85**, 2589 (2004).
23) R. Carpenter, N. Cramp, and K. O'Grady, IEEE Trans. Magn. **48**, 4351 (2012).
24) X.-Y. Yuan, X.-B. Xue, L.-F. Si, J. Du, and Q.-Y. Xu, Chin. Phys. Lett. **29**, 097701 (2012).
25) J. Lee, S. Kim, C. Yoon, C. Kim, B. Park, and T. Lee, J. Appl. Phys. **92**, 6241 (2002).
26) K.-Y. Kim, H.-C. Choi, C.-Y. You, and J.-S. Lee, J. Appl. Phys. **105**, 07D715 (2009).
27) J. van Lierop, K. W. Lin, H. Ouyang, Y. M. Tzeng, and Z. Y. Guo, J. Appl. Phys. **99**, 08C104 (2006).
28) K.-W. Lin, R. Gambino, and L. Lewis, J. Appl. Phys. **93**, 6590 (2003).
29) M. Caminale, R. Moroni, P. Torelli, G. Panaccione, W.-C. Lin, M. Canepa, L. Mattera, and F. Bisio, Phys. Rev. B **91**, 094435 (2015).
30) G. Han, B. Zong, P. Luo, and Y. Wu, J. Appl. Phys. **93**, 9202 (2003).
31) K.-W. Lin, H.-R. Huang, H.-F. Hsu, Y.-C. Yang, J.-Y. Guo, T. Suzuki, and J. van Lierop, 3rd Int. Nanoelectronics Conf. (INEC), 2010, p. 1171.